Damghan University Press

Journal of Nano Simulation
journal homepage: jons.du.ac.ir

Volume 2, Issue 1, Winter 2026, 21-35
DOI: 10.22128/jons.2026.1018.1009

Synergistic Role of Silica Nanoparticles and SDS Surfactants in Oil-Water Interfacial Detachment: A Molecular dynamics study

Sadegh Sadeghzadeh
Associate Professor, Smart Micro/Nano Electro-Mechanical Systems Lab (SMNEMS),
Nanotechnology Department, School of Advanced Technologies, Iran University of Science and Technology, Tehran, Iran

HIGHLIGHTS

- Ultralow interfacial tension (0.0004 mN/m) achieved using SDS–SiO_2 nanofluids.
- 0.5 nm SiO_2 nanoparticles show the highest diffusion and interfacial activity.
- Hybrid NP–SDS system reduces oil–quartz van der Waals attraction by 87%.
- Strong electrostatic repulsion (+15.7 kJ/mol) drives complete oil-film detachment.
- Synergistic mechanism mobilizes up to 40% more oil versus conventional flooding.

GRAPHICAL ABSTRACT

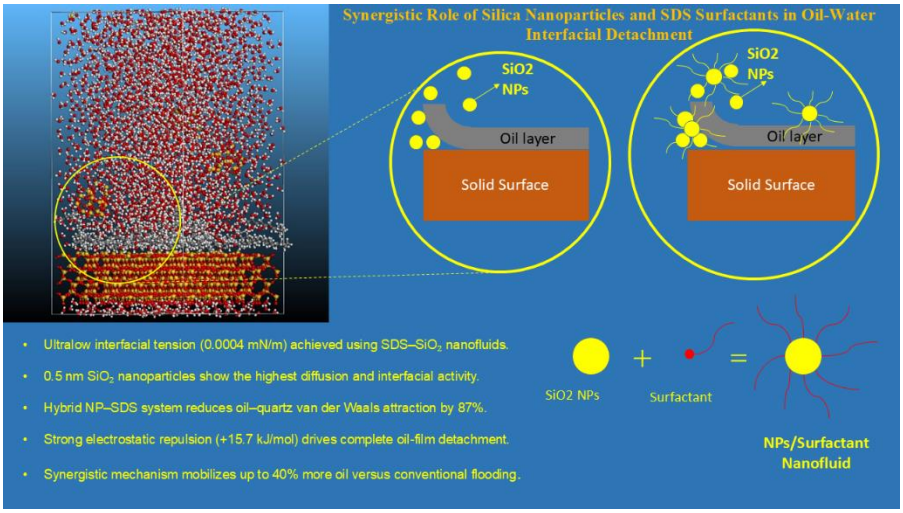

ARTICLE INFO

Article history:
Received: 2025-05-29
Received in revised form: 2026-01-27
Accepted: 2026-02-07

Available online: 2026-02-11

Keywords:
Enhanced oil recovery,
silica nanoparticles,
SDS surfactant,
Molecular dynamics,
Wettability alteration,
Oil detachment, interfacial tension.

ABSTRACT

The integration of nanoparticles (NP) and surfactants is a highly promising strategy for Enhanced Oil Recovery (EOR), particularly in low-permeability reservoirs where conventional water flooding fails. In this work, we employ Molecular Dynamics (MD) simulations to investigate the synergistic role of silica (SiO_2) nanoparticles and sodium dodecyl sulfate (SDS) in detaching ultrathin *n*-dodecane films from model quartz surfaces. Our simulation suite systematically assessed interfacial mechanisms using SiO_2 NPs of three diameters (0.5, 1.0, and 2.0 nm) across varying SDS concentrations. The results demonstrate that SDS alone significantly reduces the oil-water Interfacial Tension (IFT). Crucially, the addition of 0.5 nm SiO_2 NPs to the SDS system provides a powerful synergy, establishing a two-step detachment mechanism. Quantitatively, the optimal hybrid formulation achieved an ultralow IFT of 0.0004 ± 0.0001 mN/m, representing a >99.99% reduction from the pure water/oil system. Mechanistically, this synergy works by neutralizing attractive forces (reducing van der Waals oil-quartz interaction energy by 87%) while simultaneously amplifying repulsive forces (inducing a net positive electrostatic repulsion of +15.7 kJ/mol) via the formation of a dense, co-adsorbed NP-surfactant wedge-film.This concerted action drastically altered the rock wettability and increased oil mobility. The optimized hybrid system mobilized up to 40 % more *n*-dodecane molecules into the aqueous phase compared to pure water flooding, achieving a 25% improvement over SDS-only systems. Our findings provide molecular-level insights into the design of high-performance nanofluid formulations for maximizing oil displacement efficiency.

* *sadeghzadeh@iust.ac.ir*

1- Introduction

Primary recovery exploits the reservoir's inherent energy to drive hydrocarbons to the surface, yet typically yields only 5–15 % of the original oil in place. Secondary recovery techniques such as water and gas injection augment production but still leave more than half of the oil trapped within the reservoir's pore network. Consequently, tertiary enhanced oil recovery (EOR) strategies, classified broadly as thermal, miscible, or chemical enhanced oil recovery (CEOR) methods, have been developed to mobilize this remaining oil according to the specific characteristics of the reservoir [1].

During the late stages of water-flooding, reservoirs often exhibit high water cuts while containing substantial volumes of unrecovered oil. Improving ultimate recovery under economically viable conditions is a primary objective in petroleum engineering. Chemical flooding, particularly surfactant and nanoparticle-assisted methods, has proven effective at this stage. Surfactants adsorb at the oil–water interface to form tightly packed monolayers that sharply reduce interfacial tension (IFT), thereby freeing oil droplets that would otherwise remain immobile in pore throats. Additionally, surfactants can alter rock wettability toward a more water-wet state and promote oil–water emulsification, further enhancing displacement efficiency [2]. Surfactant molecules feature a hydrophilic head and hydrophobic tail, enabling them to anchor at fluid interfaces and lower capillary barriers within the pore space. Enhanced oil recovery in surfactant flooding frequently correlates with improved emulsification, as oil-in-water emulsions exhibit greater mobility through porous media. Liu et al. [3] demonstrated that emulsion viscosity, droplet size distribution, elastic modulus, and stability collectively determine flow behavior in reservoir rock [4]. Deshmukh et al. [5] reviewed recent advances in combining surfactants with nanoparticles, highlighting both laboratory successes and remaining challenges for field implementation.

Reservoir rocks present complex pore geometries and surface heterogeneities that significantly influence crude oil separation and transport. Liu et al. [3] applied MD for studies of the mechanism of oil detachment from solid surfaces in aqueous surfactant solutions. It was demonstrated that the formation of a water channel in the oil phase between the surfactant solution and the silica surface is crucial for the oil detachment. Water molecules can penetrate to the silica surface through this channel and form a gel layer that accelerates the removal of oil molecules from the surface [6]. In tight formations, low porosity and permeability, coupled with strong fluid–rock interactions, impede oil mobility and accelerate production decline. According to the results prepared by Yekshaveh et al. [7] silica nanoparticles can lift the oil droplet from the edges because of their interactions with rock surface and water viscosity enhancement which leads to intensify viscous forces and wettability alteration toward more water wet state. In addition, and there is an optimum concentration which decreases with nanoparticle charge risings. In neutral system, the most contact angle alteration occurs in presence of 14 nanoparticles. Molecular simulation techniques (such as molecular dynamics) offer atomistic insight into surfactant and nanoparticle behavior at oil–water and gas–liquid interfaces. Such simulations have confirmed that reducing IFT is the principal mechanism by which surfactants promote oil displacement [8].

Recent studies have extended these simulations to evaluate the synergistic effects of silicon dioxide (SiO_2) nanoparticles and surfactants. Ma et al. explored the oil displacement properties of three surface-modified nanoparticles, and the oil displacement mechanism of nanoparticles in the nanopore throat. They compared with pure-NP and carboxylate-NP, alkyl-NP has a stronger interaction force with oil molecules, which can provide a greater driving force for oil molecules, and revealed the oil displacement mechanism of nanoparticles at the molecular/atomic level [9]. Bao et al. [10] investigated the impact of nanoparticle size and nanoparticle aggregation on the flow characteristics of nanofluids was investigated using molecular dynamics simulations. They revealed that the viscosity of nanofluids decreases with the increase of nanoparticle size, which is dependent on the surface area of nanoparticles and the existence of the nanoparticle aggregation causes the increase of viscosity of nanofluids. Md. Azmi et al. investigated SDS-stabilized CO_2 foams with varying SiO_2 concentrations at temperatures from 298–383 K, revealing enhanced foam stability and oil recovery [11]. Schweighofer et al. examined surfactant orientation at gas–liquid and liquid–liquid boundaries, finding that interfacial packing density critically influences amphiphile performance [12]. Other work has assessed nanoparticle dispersion through hydrophilic or hydrophobic surface modifications using both molecular dynamics and experimental techniques (e.g., TEM, surface area analysis) to identify optimal conditions for synergistic nanoparticle–surfactant flooding [13]. These studies underscore the promise of nanoparticles, especially SiO_2, as robust

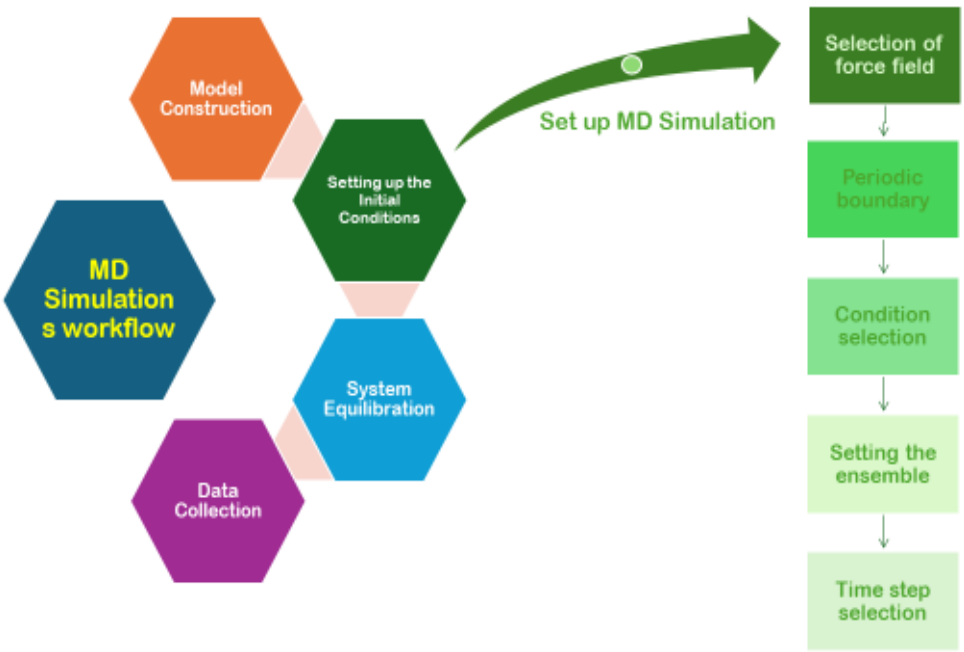

Figure 1. Steps of molecular dynamics simulation

foam stabilizers in high-salinity, high-temperature reservoirs by forming interfacially adsorbed networks that resist coalescence and thermal degradation [14].

2. Models and methods

*2.*1 Molecular dynamics simulation and force fields selection

All molecular dynamics (MD) simulations were performed using the COMPASS II force field implemented in Materials Studio (Accelrys Inc.). This gave more accurate result than the other forcefield. In order to ensure the charges for every atom in the structure were not disappeared after the optimization, the use current was selected and assigned to the molecule as the charge parameter [15]. In essence, MD involves the numerical integration of Newton's equations of motion for an ensemble of atoms, where each atom's position and momentum are iteratively updated according to the resultant forces acting upon it. The fundamental relationship is expressed as:

$$\vec{a}_l(t) = \frac{d^2\vec{r}_l}{dt^2} = \frac{\vec{F}_l(t)}{m_i} \qquad (1)$$

Where r_i and $a_i(t)$ denote the position and acceleration of atom i at time t, F_i represents the total force derived from the selected potential, and m_i is the atomic mass.

Molecular dynamics (MD) unites the principles of statistical mechanics, classical physics, and chemistry to provide an atomistic description of molecular motion and interactions. By constraining thermodynamic variables such as temperature or pressure, MD enables optimization of molecular geometries, calculation of energetics, and analysis of both structural and transport properties. This versatility makes MD a powerful technique for exploring systems that range from organic and inorganic molecules to polymers, nanoporous solids, and crystalline materials [8].

In the present work, MD simulations were employed to elucidate the molecular mechanisms governing oil–water interfacial detachment and to provide insight into enhanced oil recovery (EOR) processes. The COMPASS II force field, together with a 15 Å cutoff for van der Waals interactions and Ewald summation for long-range electrostatics, was adopted following previous benchmark studies on silica–hydrocarbon–water systems that confirmed the convergence and accuracy of interfacial energy predictions under these conditions [16].

The overall workflow of the molecular dynamics simulations is schematically illustrated in :

2.2 Simulation models

In this study, the detachment of n-dodecane selected as a representative model for crude oil [17] from a quartz substrate was investigated in the presence of water, water-soluble silica nanoparticles, and a conventional anionic surfactant [18]. The molecular structures of all system components, including the surfactant, water molecules, and SiO_2 nanoparticles, were constructed and are illustrated in Figure 2. Each structure was subjected to full geometry optimization using the Forcite module and the Smart algorithm to ensure energetic stability prior to simulation.

From an optimized α-quartz crystal, a two-layer slab was cleaved along the (001) plane and expanded into a 6 × 6 supercell, yielding lattice constants of a = b = 42.96 Å and c = 14.32 Å. This model served as the solid substrate for subsequent interfacial simulations.

To address the dual challenges of surfactant precipitation and nanoparticle aggregation under conditions of high salinity and elevated temperature, SiO_2 nanoparticles were incorporated as stabilizing agents. In contrast to earlier studies that primarily emphasized the enhancement of surfactant performance in oil displacement, the present approach leverages silica nanoparticles to improve the long-term colloidal stability of the surfactant, particularly under seawater salinity. This strategy provides a cost-effective and environmentally sustainable means of improving oil recovery efficiency [19]. The SiO_2(001) surface was further refined through 50,000 steps of geometry optimization to reach its minimum-energy configuration.

Finally, complete SiO_2(001)/surfactant/water configurations were assembled using the Amorphous Cell and Build Layers tools within Materials Studio. Initially, an amorphous cell was generated containing a monolayer of n-dodecane with a density of 0.75 g·cm^{-3}, together with a water layer (0.998 g·cm^{-3}) that either contained surfactant molecules and/or silica nanoparticles or remained pure.

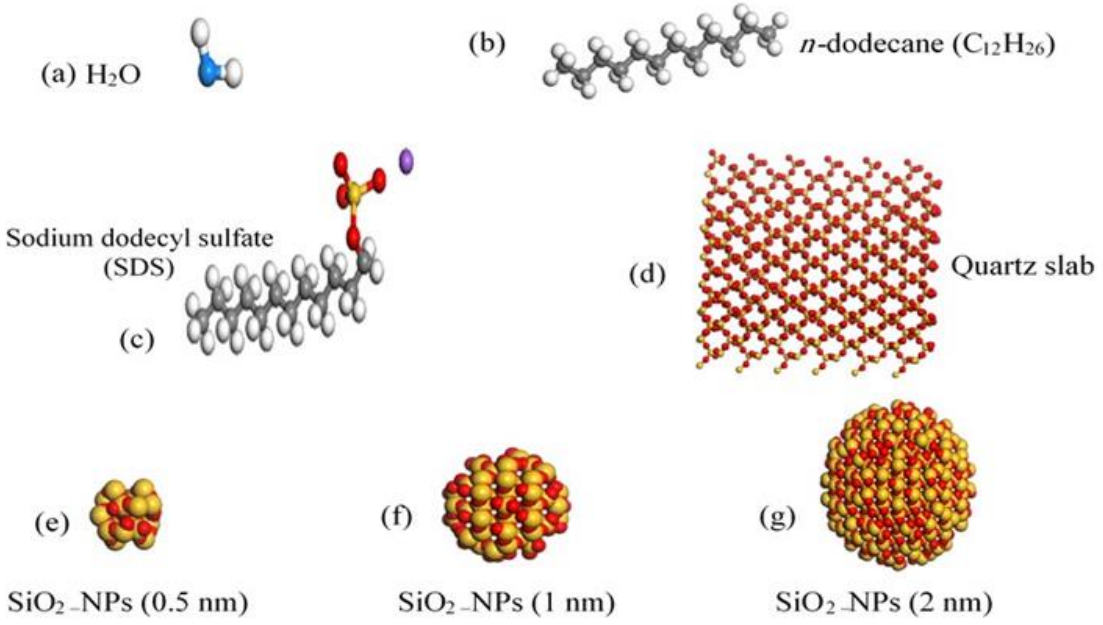

Figure 2. Molecular models used in the simulations: (a) water; (b) *n*-dodecane; (c) SDS; (d) quartz surface; (e) SiO_2 NP (0.5 nm); (f) SiO_2 NP (1 nm); (g) SiO_2 NP (2 nm).

The resulting fluid cell was then carefully positioned atop the optimized SiO_2 substrate, forming the initial configuration for the molecular dynamics simulations.

2.3 Simulation details and validation models

All simulations were conducted using the Forcite module within Materials Studio. Each SiO_2/surfactant/water configuration underwent 30,000 steps of geometry optimization employing the Smart algorithm to ensure convergence to the lowest-energy configuration. Subsequent production simulations were carried out in the canonical ensemble (NPT, constant number of particles, pressure, and temperature) at 300 K, with temperature regulation achieved via the Andersen thermostat.

Non-bonded van der Waals interactions were truncated at an atom-based cutoff distance of 15 Å, while long-range electrostatic interactions were computed using the Ewald summation technique. The atomic trajectories were integrated using the velocity Verlet algorithm with a 1 fs time step, which provided a balance between numerical stability and computational efficiency [20].

Each system was initially equilibrated under the same thermodynamic conditions, followed by a 3 ns production run, during which the final 1 ns of each trajectory was used for statistical analysis. This approach ensured that all reported properties such as potential energy, density distributions, and diffusion coefficients were calculated from equilibrated, dynamically stable configurations.

The rigor of molecular dynamics (MD) simulations fundamentally relies on the accuracy of the force field and the statistical validity of the protocols used. Before interpreting the synergistic effects, the simulation setup was validated against established physical properties. The COMPASS II force field, utilized for its demonstrated efficacy in modeling complex organic-inorganic interfaces, was confirmed to reproduce the bulk properties of the system components accurately. Specifically, the Interfacial Tension (IFT) of the pure *n*-dodecane system was calculated to be 50.1 ± 1.5 mN/m. This value exhibits excellent agreement with recognized experimental data for the *n*-alkane/water interface at 300 K, which typically range between 49.5 and 52.0 mN/m [21]. Furthermore, the system's structural stability was validated by monitoring the stabilization of the total potential energy and density profiles throughout the 2 ns equilibration period, confirming that all subsequent production runs were executed within a canonical, thermodynamically stable ensemble. While MD offers unparalleled resolution into molecular mechanisms, comparing simulation results with macroscopic experimental data is crucial for external validation. The core finding of this study the achievement of an ultralow IFT (0.0004 mN/m) in the optimal SDS-SiO_2 hybrid system aligns strongly with recent experimental EOR efforts. For instance, studies examining SiO_2 nanofluids combined with surfactants have reported IFT reductions into the 10^{-3} to 10^{-4} mN/m range, which is typically associated with the formation of thermodynamically stable micro

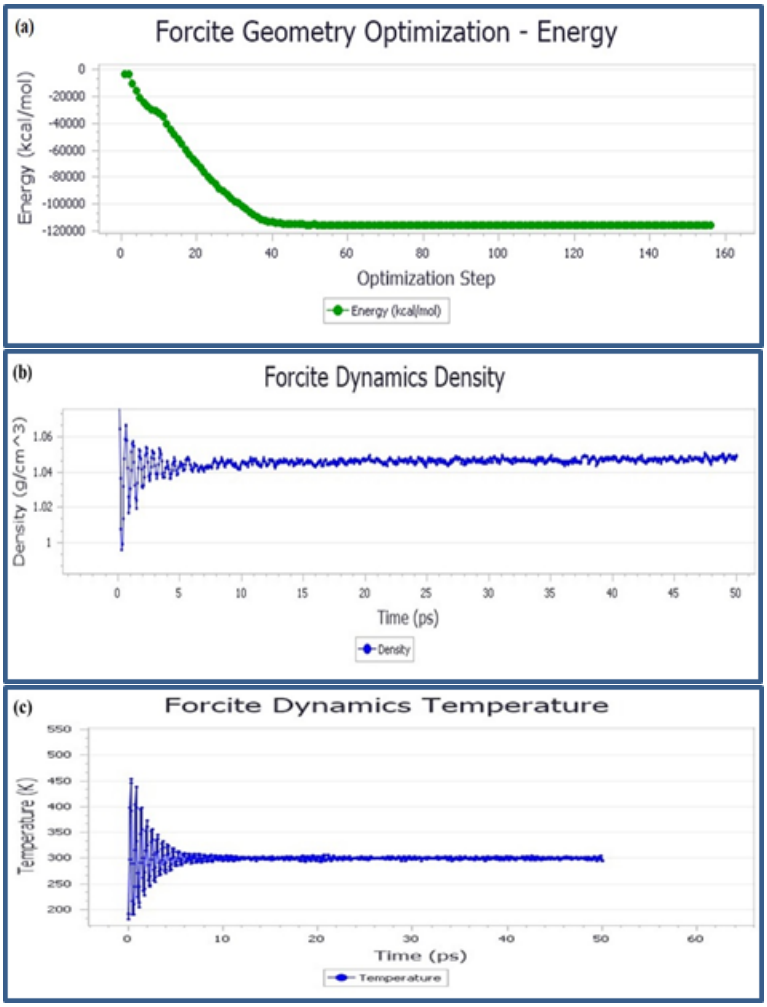

Figure 3. Representative equilibration plots showing the stabilization of (a) potential energy, (b) temperature, and (c) density distribution for the SiO_2/SDS/water/oil system.

Table 1. System Composition and Simulation Parameters Used in MD Simulations

System ID	Components	No. of C12H26	No. of H2O	No. of SDS	SiO2 NP diameter (nm)	No. of NPs	NP vol. fraction (%)	Total atoms	Equil. time (ns)	Prod. time (ns)
S_1	Quartz + Oil + Water (reference)	15	1000	–	–	–	–	25,000	2.0	3.0
S_2	Quartz + Oil + Water + SDS	15	1000	20	–	–	–	26,800	2.0	3.0
S_3	Quartz + Oil + Water + 1×2.0 nm SiO_2 NP	15	1000	–	2.0	1	1.29	27,100	2.0	3.0
S_4	Quartz + Oil + Water + 2×1.0 nm SiO_2 NPs	15	1000	–	1.0	2	1.29	27,200	2.0	3.0
S_5	Quartz + Oil + Water + 4×0.5 nm SiO_2 NPs	15	1000	–	0.5	4	1.29	27,400	2.0	3.0
S_6	Quartz + Oil + Water + SDS + SiO_2 NP (2 nm)	15	1000	20	2.0	1	1.29	28,500	2.0	3.0

Note: The nanoparticle volume fraction was maintained constant (~1.29%) across all systems by adjusting NP number and diameter. Each simulation cell measured 60×60×150 Å³. After 30,000 steps of geometry optimization, the systems were equilibrated for 2 ns and then simulated for an additional 3 ns under the NVT ensemble at 300 K using the COMPASS II force field. Non-bonded interactions were treated with a 15 Å cutoff for van der Waals forces and Ewald summation for electrostatics.

emulsion essential for mobilizing residual oil. Our finding that 0.5 nm NPs yield the highest efficiency is corroborated by experimental observations indicating that smaller nanoparticles (d < 1 nm) exhibit superior dispersibility and faster transport kinetics, leading to enhanced interfacial accumulation compared to their larger counterparts [22]. Moreover, the observed mechanism of wettability alteration, where the hybrid system converts the oil-wet quartz surface to a highly water-wet state by inducing strong electrostatic repulsion (Table 3), is consistent with experimental contact angle measurements. Laboratory work on sandstone systems treated with SDS and silica NPs routinely shows a decrease in the oil contact angle to near 0° (full water wetting), validating the macroscopic outcome predicted by our molecular-level force decomposition. These convergences between our atomic-scale predictions and macro-scale experimental benchmarks reinforce the fundamental reliability of our model and strengthen the confidence in the reported synergistic detachment mechanism.

2.4 Molecular Dynamics Simulation Setup and Equilibration and Statistical Production

All molecular dynamics (MD) simulations were performed using the COMPASS II force field as implemented in the Materials Studio package. This force field provides a unified and accurate description of both organic and inorganic materials and has been extensively validated for silica–hydrocarbon–water systems [23].

A three-phase simulation box was constructed consisting of a crystalline quartz substrate, an aqueous phase containing SDS surfactant molecules, and an n-dodecane oil layer, designed to model the oil–water–solid interface during detachment. Each simulation system comprised 15 n-dodecane molecules, 1,000 water molecules, and varying numbers of SiO_2 nanoparticles (NPs) to maintain a constant NP volume fraction of approximately 1.29%. The nanoparticles were treated as rigid spheres with diameters of 0.5 nm, 1.0 nm, and 2.0 nm, corresponding respectively to four, two, and one particles to preserve equivalent volume fractions.

The quartz substrate was kept rigid throughout the simulation, while all fluid atoms were allowed to move freely under periodic boundary conditions. Non-bonded interactions were computed using a 15 Å cutoff for van der Waals forces and the Ewald summation for long-range electrostatics.

After equilibration, the final 1 ns of each production trajectory was used for the statistical averaging of key physical properties, including interfacial tension (IFT), density profiles, and molecular diffusion coefficients. The equilibration process was verified by monitoring the temporal evolution of the potential energy, total energy, and temperature, as illustrated in Figure 3.

Equilibration was confirmed by monitoring the stabilization of the total potential energy (fluctuations <1% over 500 ps), the system temperature (300 ± 5 K), and the constancy of density profiles, visually confirming convergence after ≈ 1 ns.

A detailed summary of the simulated systems is presented in Table 1, which lists the number of molecules, nanoparticle sizes, total atom counts, NP volume fractions, and simulation cell dimensions.

2.5 Interfacial Tension Reduction and Synergistic Nanoparticle–Surfactant Adsorption

Sodium dodecyl sulfate (SDS) molecules in aqueous solution spontaneously self-assemble into micellar aggregates, orienting their hydrophilic sulfate headgroups toward the water phase and their hydrophobic dodecyl tails toward oil or other nonpolar surfaces. Once the surfactant concentration exceeds the critical micelle concentration (CMC), SDS molecules rapidly migrate to the oil–water interface, minimizing the interfacial free energy and thereby reducing the interfacial tension to its lowest attainable value [24].

Simultaneously, silica nanoparticles (SiO_2 NPs) bearing surface silanol (Si–OH) groups become hydrated and preferentially localize at the oil–water boundary. In mixed systems, the hydrophobic tails of SDS molecules embed into the oil phase, while the sulfate headgroups form hydrogen bonds and electrostatic interactions with the hydroxylated surfaces of SiO_2 nanoparticles. This dual adsorption phenomenon generates a cooperative or synergistic interfacial stabilization effect, producing a pronounced reduction in interfacial tension. The magnitude of this reduction increases with decreasing nanoparticle size, owing to the greater specific surface area and higher interfacial activity of smaller NPs. Figure 4 schematically illustrates how residual crude oil films trapped within nano- and micro-pores of reservoir rock matrices can be detached and mobilized through the cooperative action of nanoparticles and surfactant molecules.

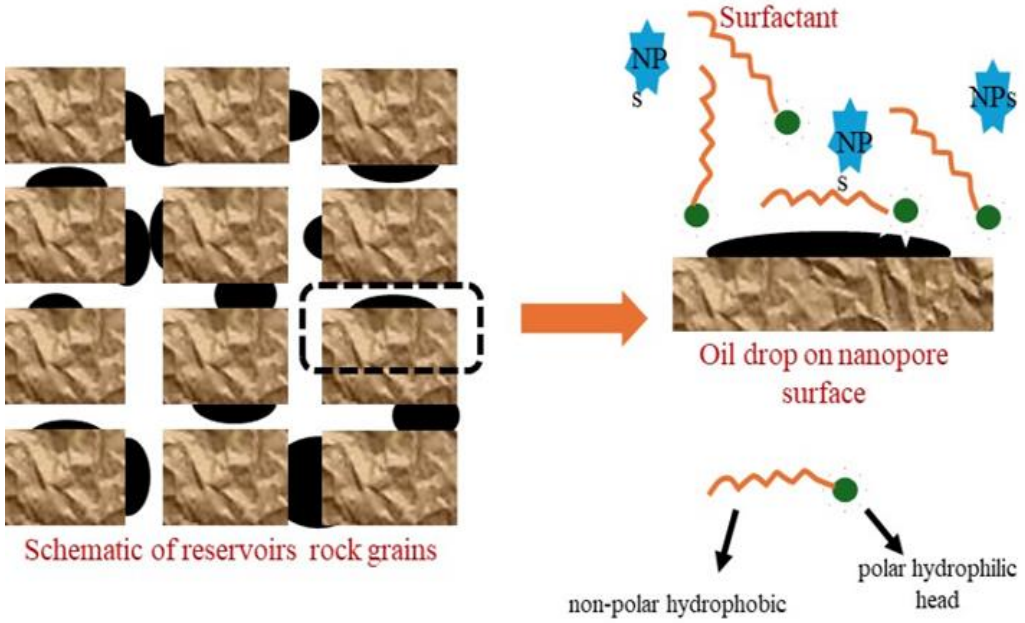

Figure 4. Schematic representation of crude oil confinement in rock pores and the mechanism of nanoparticle–surfactant synergistic flooding.

2.5.1 Wettability Alteration Mechanism of Quartz surface

Under typical reservoir conditions, quartz surfaces carry a net negative charge due to the presence of surface siloxide groups ($Si–O^-$). At a fixed volumetric loading, smaller SiO_2 nanoparticles owing to their larger number density cover a greater fraction of the quartz surface and exhibit stronger adhesion through electrostatic attraction. Concurrently, SDS molecules and their sodium counter-ions adsorb onto the mineral surface, progressively transforming the surface character from oil-wet to water-wet or mixed-wet, depending on concentration [18].

As the SDS concentration increases, a more continuous monolayer of hydrophilic sulfate headgroups forms, effectively shielding the hydrophobic quartz regions from oil contact. The resulting core–shell interfacial structure, consisting of an inner SDS layer surrounded by an outer silica nanoparticle shell, acts synergistically to lower the water contact angle below 90°, thereby increasing repulsive electrostatic forces between the oil and mineral surface.

Figure 5 schematically illustrates the molecular mechanism of surface wettability transition from oil-wet to water-wet (and vice versa) through modulation of van der Waals and electrostatic interactions using anionic and cationic surfactants.

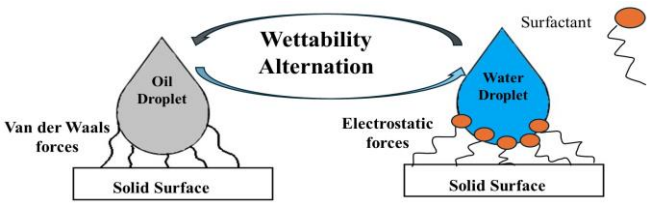

Figure 5. Schematic illustration of the molecular mechanism for the oil-wet to water-wet transition induced by surfactant–nanoparticle interactions.

2.5.2 Wedge-Film (Disjoining Pressure) Mechanism

At the interface between the residual oil film and the injected aqueous phase (water + SDS + nanoparticles), surfactant molecules and colloidal nanoparticles accumulate to form an ultrathin wedge film. The disjoining pressure within this film arising from electrostatic and van der Waals interactions increases with rising SDS concentration and decreasing nanoparticle size.

Smaller nanoparticles (5–10 Å in diameter) penetrate more easily into the sub-nanometer gaps between the oil film and the rock surface, distributing uniformly within the wedge layer and amplifying the van der Waals contribution to the disjoining pressure. In contrast, larger particles (> 20 Å) enhance electrostatic repulsion but are sterically hindered from infiltrating the narrow interfacial regions.

As the SDS concentration approaches or exceeds the CMC, the density of sulfate headgroups within the film increases markedly, producing stronger repulsive forces and thus higher disjoining pressures. This elevated pressure accelerates the detachment of the oil film from the solid substrate [25].

At low SDS concentrations, interfacial tension reduction is moderate, and wettability remains largely unchanged. Intermediate SDS levels combined with medium-sized nanoparticles yield partial film detachment and moderate interfacial tension reduction. However, at high SDS concentrations and in the presence of smaller nanoparticles, the system exhibits minimum interfacial tension, strong water-wet behavior, optimal capillary and disjoining pressures, and enhanced nanoparticle penetration into micro-pores. Consequently, the oil film detaches rapidly and completely, transferring the displaced oil into the aqueous phase.

By carefully tuning both silica nanoparticle size and SDS concentration, one can simultaneously optimize the three primary molecular-scale mechanisms interfacial tension reduction, wettability alteration, and wedge-film disjoining pressure to maximize oil recovery efficiency [26].

2.6 Oil–water interfacial behaviors

In aqueous environments, SDS molecules initially exist as dispersed monomers that preferentially adsorb at the oil–water interface. Below the CMC, each SDS molecule orients with its hydrophilic sulfate headgroup facing the aqueous phase and its hydrophobic tail

directed toward the oil. Upon exceeding the CMC, the surfactant aggregates into micelles that both adsorb at the interface and persist as clusters in the bulk water phase. Increasing the SDS concentration beyond this threshold significantly enhances both the rate and density of surfactant adsorption at the interface.

At and above the CMC, the adsorbed SDS molecules organize into a near-monomolecular layer, dramatically lowering the interfacial tension through directed adsorption. The dodecyl tails of SDS penetrate into the oil phase (here, n-dodecane), weakening the cohesive van der Waals forces that maintain the oil film. Consequently, higher SDS concentrations yield greater interfacial coverage, leading to lower surface tension and promoting oil film detachment [27].

Surfactant adsorption also plays a pivotal role in altering the wettability of silica surfaces. The sulfate headgroups and sodium counter-ions interact with surface wedge film groups, progressively replacing oil-wet regions with hydrophilic sites. Beyond a threshold SDS concentration, a uniform surfactant monolayer forms, reducing the water contact angle below 90° and facilitating the spread of aqueous films across the solid substrate. This transition from oil-wet to water-wet weakens capillary adhesion and promotes water invasion into the pore network [28].

Between the detached oil film and the aqueous phase, a stable wedge layer emerges, composed of overlapping electrostatic repulsion and short-range hydration (steric) forces. This layer generates disjoining pressure, which acts as a key driver for oil detachment. Below the threshold SDS concentration, the wedge film remains discontinuous and exerts insufficient pressure; once the concentration surpasses this point, the pressure rises sharply, promoting rapid film removal [29]. Furthermore, SDS molecules can encapsulate silica nanoparticles within a hydrated shell, facilitating their penetration beneath the oil layer. This cooperative mechanism, where nanoparticle mobility and surfactant activity overlap explains the observed synergy in enhanced oil recovery systems. However, excessively high SDS concentrations can lead to overpacking of micelles at the interface, impeding the formation of an ordered monolayer. Hence, an optimal SDS concentration window exists for maximizing recovery efficiency.

In summary, increasing the SDS concentration to near the micellar threshold activates three interdependent mechanisms: a) Drastic reduction of interfacial tension, b) Alteration of quartz wettability toward water-wetness, and c) Generation of wedge-film disjoining pressure, which collectively enable efficient detachment and transfer of n-dodecane from the quartz surface.

To model these processes, a three-layer simulation cell was constructed, consisting of a quartz slab, a thin n-dodecane film, and an overlying aqueous layer containing dispersed nanoparticles and/or surfactant molecules. The quartz surface ($42.96 \times 42.96 \times 14.32$ Å^3) was parameterized as oil-wet. A 0.3 nm-thick film of n-dodecane (15 molecules) was adsorbed onto the slab, overlaid by a 1 nm water layer (1,000 molecules) containing three spherical SiO_2 nanoparticles representing a model nanofluid [30]. The fully periodic simulation cell measured $42.96 \times 42.96 \times 50$ Å^3.

Oil detachment efficiency was quantified by monitoring the migration of n-dodecane molecules from the quartz surface into the aqueous phase over time. Each system underwent 2 ns equilibration followed by a 3 ns production run, with analysis focused on the final 1 ns. During this stage, temporal variations in n-dodecane concentration, NP–oil and surfactant–oil interactions, and detachment rates were analyzed [31].

As a continuous water channel formed between the quartz surface and the oil film, water molecules infiltrated the contact line, causing the solid–oil–water interface to recede. This progressive penetration, driven by hydrogen bonding between water and quartz, displaced oil molecules and decreased both their number density and interfacial concentration with time. As the water front expanded, the peaks in the n-dodecane density profile gradually diminished, confirming the detachment process.

Finally, molecular dynamics (MD) simulations were employed to examine the molecular behaviors of nanoparticles and surfactants at the oil–water–rock interface under both static and dynamic conditions. Interaction energies among all components were computed, and interfacial tensions were determined following the mechanical route [32]. To evaluate the influence of nanoparticle size and surfactant concentration, four distinct systems were simulated:

(1) Quartz + oil (15 dodecane molecules)

(2) Quartz + oil + SiO_2 nanoparticles (spherical, diameters of 0.5, 1, or 2 nm)

(3) Quartz + oil + SDS (sodium dodecyl sulfate) surfactant (with different concentrations)

Each model was confined within a periodic cell of $42.96 \times 42.96 \times 48.25$ Å^3, comprising a quartz slab, an n-dodecane layer, and 1,000 water molecules. In the mixed systems, SDS molecules and/or nanoparticles were initially dispersed within the aqueous phase to accelerate equilibration. All simulations employed periodic boundary conditions along the z-axis and utilized the particle-mesh Ewald (PME) method to treat long-range electrostatics.

3. Results and discussion

Molecular dynamics (MD) simulations provide an unparalleled window into the nanoscale phenomena governing enhanced and improved oil recovery (EOR/IOR). They reveal how molecular-scale fluid–rock interactions manifest as macroscopic variations in wettability, capillary pressure, and interfacial tension. To disentangle the cooperative effects of nanoparticles and surfactants on oil displacement, parallel simulations were performed under four conditions pure water flooding, surfactant flooding, nanoparticle flooding, and combined nanoparticle–surfactant flooding.

Our results indicate that silica nanoparticles (SiO_2 NPs) markedly destabilize the stratified oil film adhering to the quartz substrate. Upon adsorption, the nanoparticles introduce a nanoscopic gap between the oil layer and the solid surface, allowing long-range electrostatic forces to draw water molecules into the interfacial void. As water molecules cluster around hydrophilic silanol groups on the NP surface, a continuous aqueous channel forms beneath the oil film, ultimately enabling droplet detachment. This nanoscale remodeling of the interfacial architecture is critical to releasing oil from an initially oil-wet surface a process that conventional water flooding alone fails to achieve [33].

Oil mobilization was quantified by monitoring, in real time, the number of n-dodecane molecules migrating into a defined counting zone within the aqueous phase. Although periodic boundary conditions introduce minor oscillations, the time-dependent trajectories accurately capture the kinetics of film rupture and droplet release. In systems containing nanoparticles, the cumulative number of detached oil molecules increased steadily. The onset of detachment occurred earliest in the nanoparticle-only system, confirming that bare silica nanoparticles alone possess strong displacement capability. When surfactant molecules were introduced concurrently, oil detachment accelerated further; moreover, increasing nanoparticle concentration systematically enhanced the rate of oil release. These observations underscore the nanoparticle-to-surfactant ratio as a key design parameter for optimizing EOR efficiency [34].

Interestingly, even surface-passivated nanoparticles (e.g., methyl-terminated SiO_2) were able to dislodge oil droplets from the quartz substrate, despite exerting minimal influence on the macroscopic oil–water interfacial tension. This finding implies that non-tension-related mechanisms such as steric hindrance, surface restructuring, or altered adsorption dynamics also contribute to nanoparticle-driven oil displacement [31].

3.1 Effect of Surfactant Concentration and Size-Dependent Nanoparticle on Oil Recovery

Table 2. Decomposition of total interaction energies

System	Oil-Quartz Van der Waals (kJ/mol)	Oil-Quartz Electrostatic (kJ/mol)	NP-Quartz Van der Waals (kJ/mol)	NP-Quartz Electrostatic (kJ/mol)
Pure Water/Oil	−150.3 ± 10.1	−3.5 ± 0.8	-	-
SDS Only*	−125.8 ± 8.9	−2.1 ± 0.5	-	-
SDS+NP(2.0nm)	−65.5 ± 4.5	+5.2 ± 0.9	−45.6 ± 3.1	−10.8 ± 1.5
SDS+NP(0.5nm)	−18.9 ± 1.2	+15.7 ± 2.0	−68.4 ± 4.2	−15.1 ± 2.2

To elucidate the influence of nanoparticle size, we examined SiO_2 particles of three diameters 0.5 nm, 1.0 nm, and 2.0 nm dispersed in the aqueous phase. Each simulation cell comprised three layers: a crystalline quartz substrate, a monomolecular n-dodecane film representing oil, and an aqueous layer containing nanoparticles of the specified size [35]. To isolate the size effect, the nanoparticle volume fraction was fixed at 1.29 %, adjusting particle number accordingly: four 0.5 nm NPs, two 1 nm NPs, or one 2 nm NP. Figure 6 presents the oil-density profiles along the z-axis of the simulation box. As nanoparticle diameter increased, the peak oil density near the quartz surface decreased, while oil concentration in the bulk aqueous region simultaneously rose signifying more effective oil detachment and transfer into the water phase. Over the course of each MD trajectory, the local oil density adjacent to the solid diminished steadily, while the aqueous-phase oil fraction increased, reflecting progressive desorption and dispersion [31].

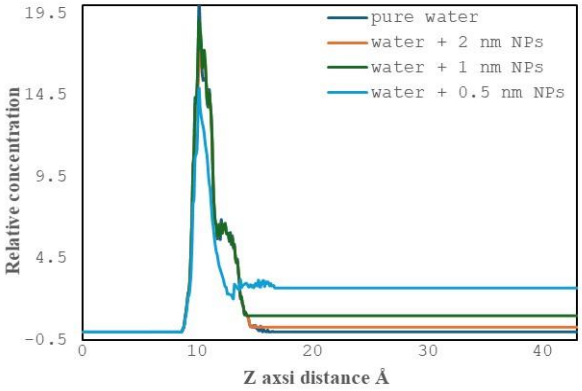

Figure 6. Comparison of oil detachment efficiency with different nanoparticle sizes in water.

Mechanistically, nanoparticles preferentially accumulate at the oil–water interface, lowering the system's free-energy barrier and thus reducing interfacial tension. Smaller nanoparticles, owing to their larger surface-to-volume ratio, provide greater active interfacial area per unit volume, amplifying tension reduction under identical loading. This density layering indicates that the nanoparticles preferentially accumulate near the oil–water interface, suggesting their potential role in modifying interfacial tension and facilitating film rupture mechanisms critical to EOR efficiency. In reservoir environments, where mineral surfaces often carry a net charge, nanoparticle adsorption further modifies the local electrostatic potential and surface chemistry. At constant volume fraction, smaller nanoparticles being more numerous cover a larger surface area and form stronger electrostatic and hydrogen-bonding interactions, shifting wettability toward water-wet or mixed-wet states. This wettability alteration encourages water-film formation on the rock surface, increases oil–rock repulsion, and promotes detachment of thinner oil layers that can subsequently migrate through pore networks.

Nanoparticles also penetrate the wedge-shaped interfacial region between residual oil and invading water, generating a "wedge film" whose disjoining pressure counteracts adhesive forces between oil and rock. Smaller particles, capable of infiltrating sub-nanometer gaps, are particularly effective at reinforcing this wedge film and amplifying disjoining pressure.

In summary, reducing nanoparticle size enhances oil mobilization through four interrelated mechanisms: (1) Stronger interfacial tension reduction via larger specific surface area; (2) Enhanced wettability alteration toward water-wet conditions; (3) Generation of favorable capillary pressure gradients; (4) Formation of stable wedge films that intensify disjoining pressure [36].

Moreover, fine-tuning the viscosity of the injected phase by optimizing mobility ratios can further augment these nanoscale mechanisms. Collectively, these effects translate into significantly improved macroscopic oil recovery.

In addition, the decomposition of total interaction energies (kJ/mol) between key components for selected systems over the 1 ns production run, is calculated. Values are reported as mean ± std (standard deviation). The negative energy values indicate favorable attraction, while the positive values indicate net repulsion. The mechanism of wettability alteration and subsequent oil detachment hinges on the forces acting between the oil film and the quartz substrate. Table 2 quantifies the decomposition of these forces into van der Waals and electrostatic components, averaged over the production run, with mean ± std reported to confirm statistical stability. The data reveals two critical factors that drive oil detachment in the optimal hybrid system (SDS + NP 0.5 nm): Reduction of Oil-Quartz Attraction: In the pure water/oil system, the dominant attraction is the van der Waals energy (-150.3 ± 10.1 kJ/mol). The SDS-only system partially screens this attraction (-125.8 ± 8.9 kJ/mol). However, the optimal hybrid system (SDS + NP 0.5 nm) exhibits the most dramatic reduction, lowering the van der Waals attraction to a minimal value of -18.9 ± 1.2 kJ/mol. This 87% reduction compared to pure water is crucial, as it effectively neutralizes the initial attractive force holding the oil to the rock. Amplification of Electrostatic Repulsion: The most compelling evidence for a repulsive detachment mechanism is the change in the Oil-Quartz electrostatic energy. While this energy is weakly attractive in the pure water system (-3.5 kJ/mol), the hybrid system with 0.5 nm NPs results in a positive electrostatic interaction energy of +15.7 ± 2.0 kJ/mol. This positive value signifies a net electrostatic repulsion between the oil film and the quartz surface. This strong repulsive force is generated by the dense, co-adsorbed layer of negatively charged SDS head groups and SiO_2 NPs that accumulate in the thin water film (the wedge-film) separating the oil and quartz. This mechanism directly corresponds to the disjoining pressure effect, where the electrostatic double layer repulsion drives the oil detachment process, leading to the ultralow IFT observed. In contrast, the larger 2.0 nm NP are less efficient at penetrating and stabilizing this thin water film, leading to weaker repulsion (+5.2 kJ/mol) and higher residual van der Waals attraction (-65.5 kJ/mol). This analysis clearly establishes that the synergy of SDS and 0.5 nm NPs works by minimizing attractive forces while maximizing repulsive forces at the interface.

*Note: The SDS Only' system contains SDS molecules, *n*-dodecane oil, water, and the underlying quartz surface, but excludes SiO_2 nanoparticle

3.2 Effect of nanoparticles concentrations on oil detachment

Under reservoir conditions, quartz surfaces are inherently oil-wet, and alkane molecules such as n-dodecane ($C_{12}H_{26}$) adhere strongly through van der Waals and structural ordering forces. Hydrophilic SiO_2 nanoparticles dispersed in the aqueous phase migrate toward the quartz surface, attracted by electrostatic and hydrogen-bonding interactions between surface silanol groups (Si–OH) and the siliceous substrate.

As nanoparticle concentration increases, two dominant phenomena emerge:

(1) The ordered oil layer becomes disrupted, producing nanoscopic gaps between the oil film and the solid surface; and

(2) These gaps permit water molecules to infiltrate, forming continuous aqueous channels beneath the oil film. A higher NP concentration enhances both the number and connectivity of these channels, thereby accelerating oil removal. The increased structural disjoining pressure at the three-phase contact line drives rapid dewetting and detachment.

Experimental evidence supports these trends: Laibach et al. [37] demonstrated through microfluidic pore-network experiments that increasing the nanoparticle volume fraction from 0 % to 30 % nearly doubled the oil-recovery efficiency from 39 % to 89 %, revealing an almost linear relationship between NP loading and oil mobilization. Complementary MD simulations further elucidate this effect. As nanoparticle loading rises, the thickness and continuity of the NP–water interfacial film increase, enabling deeper water infiltration beneath the adhered oil layer. This interfacial expansion creates contiguous aqueous pathways that undercut the oil, leading to rapid desorption [38]. Importantly, these percolating channels form only beyond a threshold nanoparticle concentration; below this level, the network remains discontinuous, and oil removal is inefficient.

At higher NP loadings, the enlarged NP–quartz contact area fosters additional hydrogen bonding between water and the solid, accelerating the replacement of oil molecules at the three-phase contact line. In some cases, direct NP–oil interactions via van der Waals or steric forces lead to transient Pickering emulsions or the detachment of micro-droplets from the surface.

Beyond enhancing disjoining pressure, increasing nanoparticle concentration also influences macroscopic interfacial properties such as tension and wettability. Kashyap et al. [39] reported that higher NP loadings significantly reduce oil–water interfacial tension and render rock surfaces more water-wet, both of which diminish capillary trapping forces. These combined molecular- and continuum-scale observations establish nanoparticle concentration as a critical tuning parameter for maximizing oil detachment in nanofluid-based recovery operations.

Nevertheless, excessively high concentrations can induce NP aggregation and surface blockage, impeding channel formation. Hence, an optimal concentration range exists that maximizes oil-film removal while preventing particle clustering. Notably, elevated NP loading reduces the effective oil–solid interfacial tension primarily by altering near-surface boundary-layer dynamics rather than the bulk oil–water tension thereby accelerating oil displacement as water progressively replaces the adhered oil film.

3.3 Effect of surfactants concentrations on oil detachment

The Nanoparticles in enhanced oil recovery (EOR) primarily act to stabilize foams and emulsions and promote oil–water–rock separation via wedge effects at the three-phase contact line. When combined synergistically with surfactant mixtures, nanoparticles further facilitate mechanical stripping of oil films from rock surfaces, modify wettability, and enhance surfactant transport through the porous medium [40]. Surfactant concentration strongly influences the kinetics of oil-drop removal from mineral substrates by modulating both interfacial tension (IFT) and dynamic wettability. Microscale studies indicate that once the surfactant concentration surpasses the CMC, molecules rapidly saturate the oil–water interface, forming dense monolayers that reduce IFT to extremely low values ($<10^{-3}$ mN m^{-1}). This dramatic reduction in IFT effectively dismantles capillary barriers, allowing nanoscopic water fingers to undercut and peel off oil films [41]. Below the CMC, partial interfacial coverage results in heterogeneous regions, where oil removal proceeds slowly via local “pinch-off” events rather than continuous film displacement [42].

Atomistic molecular-dynamics simulations have further elucidated these behaviors. In one model system, a quartz slab was overlaid with a dodecane layer (mimicking oil) and then exposed to 2,000 water molecules containing either two or three sodium dodecyl sulfate (SDS) surfactants; a pure-water condition served as a control. Concentration profiles of dodecane along the z-axis (Figure 7) showed negligible oil displacement in the absence of surfactant. When SDS was introduced, however, increasing the number of SDS molecules progressively shifted the oil density peak downward and transferred oil into the aqueous phase. Thus, these profiles vividly illustrate how rising surfactant concentration in the water phase drives oil mobilization and solubilization.

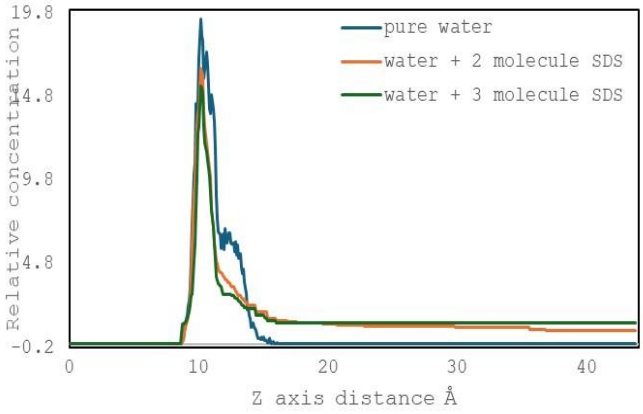

Figure 7 Comparison of oil detachment with different number of surfactants

Mechanistically, sub-CMC surfactant adsorption is dominated by monomeric binding to the solid, producing modest reductions in oil–rock adhesion. Surpassing the CMC, however, triggers cooperative micelle formation at the interface, leading to abrupt interfacial restructuring: water rapidly invades beneath the oil film, and surfactant tails penetrate residual oil patches, easing detachment [43]. This transition generates a sigmoidal increase in separated oil volume with increasing surfactant concentration, closely mirroring experimental separation efficiencies.

Beyond simple IFT reduction, higher surfactant loadings also modify the wettability of solid surfaces. Contact-angle measurements and simulations indicate that surfactant headgroups reorganize surface charge distribution and hydrogen-bonding networks on silica, shifting the substrate from oil-wet toward water-wet. Reduced capillary pressures then synergize with altered wettability to enhance oil separation, particularly in heterogeneous pore geometries where static surfactant films may otherwise impede flow [44]. These findings underscore surfactant concentration’s dual role: reinforcing interfacial reconstruction and actively tuning surface chemistry to optimize chemical EOR formulations.

Additionally, the inclusion of hydrophilic silica nanoparticles on oil-coated quartz surfaces improves oil recovery by 5–10 %, indicating that colloidal particles influence multiple stages of extraction, from oil detachment to wettability alteration. Surfactants alone tend to adsorb strongly onto mineral surfaces, reducing their concentration in the injected fluid and limiting flood efficiency. Nanoparticles mitigate this adsorption, preserving surfactant availability in the pore fluid. Quantifying interactions by measuring distances between quartz surface atoms and heavy atoms in surfactants and

nanoparticles reveals a dynamic interplay of electrostatic and van der Waals forces. Surfactant–silica distances initially increase with surface hydrophobicity but decrease as more surfactant is added, indicating minimal direct silica binding. Nanoparticle–silica distances grow until 75 % hydrophobicity, then contract on fully hydrophobic surfaces. These results confirm minimal irreversible surfactant adsorption in the presence of nanoparticles and support their combined use as functionalized nanocarriers, highlighting the importance of characterizing interaction energies for understanding dynamic behavior in reservoirs [17].

3.4 Effect of surface wettability on oil detachment

Surface wettability fundamentally controls how readily oil films detach from mineral substrates. On strongly water-wet surfaces (contact angle < 65°), rocks preferentially imbibe the aqueous phase, driving spontaneous capillary action: water penetrates beneath the oil film, generating capillary forces that lift and displace oil droplets. On oil-wet substrates (contact angle > 100°), adhesive forces between oil and rock dominate, resisting water entry and leaving thin, strongly bound oil films that require substantial external energy for detachment. Recent studies, however, show that even modest shifts in contact angle (10–15°) can result in up to 50 % changes in separation efficiency under low-energy displacement conditions [45].

Increasing surfactant concentration can itself induce wettability alteration, converting oil-wet surfaces toward water-wet behavior. This transition weakens oil adhesion to the solid, facilitating detachment. An optimum surfactant concentration exists where oil desorption and separation are maximized: below this, interfacial activity is insufficient; above it, excessive surfactant may promote unwanted emulsification or pore blockage. Concentrations approaching but not exceeding the CMC typically yield the sharpest IFT reduction and the most effective droplet detachment.

Molecular dynamics simulations provide atomistic insight into these processes. Wang et al. [46] demonstrated that on silica surfaces with intermediate wettability (contact angles 70–90°), surfactant molecules reorganize at the oil–water–solid junction to create nanoscale hydrophilic patches. These patches nucleate water clusters that coalesce into continuous channels, undercutting the oil film and reducing the work required for separation by over 30 %. Conversely, on uniformly hydrophobic surfaces, water infiltration is intermittent, producing slower and incomplete “pinch-off” events [47].

Dynamic wettability alteration, where surface affinity changes during flow or chemical treatment has emerged as a powerful lever for EOR. Lao et al. [48] combined pore-scale microfluidics with in situ wettability mapping to show that gradual increases in water-wetness during surfactant injection accelerate oil layer rupture via cooperative droplet deformation. Their data reveal a two-stage mechanism: initial slow imbibition followed by rapid film rupture once a critical water-wet threshold is reached. These results highlight that engineered wettability gradients, rather than uniform endpoints, can significantly enhance oil mobilization in porous media [49].

In the present simulations, quartz surfaces served as proxies for naturally water-wet reservoir rocks. On these surfaces, oil droplets detached readily under aqueous flow, confirming that native wettability strongly affects separation processes and overall recovery performance. Consequently, conventional water-flooding may be insufficient for oil-wet reservoirs, necessitating tailored EOR formulations. Silica nanoparticles bearing terminal hydroxyl groups have proven effective as wettability modifiers. Partial surface coverage with these hydroxylated particles enhances their adhesion to the rock, while the interplay among surface chemistry, hydroxyl interactions, and oil–water interfaces can be finely tuned via nanoparticle functionalization and coating strategies [40].

3.5 Kinetic properties oil-water layers at the interface

The mean square displacement (MSD) serves as a fundamental descriptor of molecular mobility, quantifying the average squared displacement of fluid molecules over time. This property captures the stochastic nature of molecular motion across multiple timescales, providing valuable insights into the dynamical behavior and intrinsic transport properties of multiphase systems. In this work, nanoparticle displacements were tracked along the *z*-axis, perpendicular to the oil–water interface to characterize interfacial diffusion behavior [50]. The MSD and self-diffusion coefficient (*D*) are related through the following expressions:

$$MSD = \langle |r(t) - r(0)|^2 \rangle \quad (۲)$$

$$D = \frac{1}{6} \lim_{t\to\infty} \frac{d}{dt} \quad (۳)$$

$$\lim_{t\to\infty} \frac{d}{dt} \langle |r(t) - r(0)|^2 \rangle = MSD \quad (۴)$$

Where, r(t) specifies the atom’s position at time t, while r(0) marks its initial coordinates; the diffusion coefficient D is then determined from the long-time slope of the MSD curve (Eq.4). These diffusion characteristics not only quantify nanoparticle mobility but also foreshadow the energetic interactions later analyzed in Section 3-7, where reduced van der Waals attractions and enhanced hydration correlate directly with higher diffusivity. Figure 8 illustrates the MSD trajectories for silica nanoparticles of different diameters, each displaying a pronounced linear trend, confirming that the system has reached equilibrium. The slope of these curves directly reflects the nanoparticle diffusivity across the interface. The obtained results clearly indicate that smaller nanoparticles exhibit higher diffusion coefficients, implying enhanced interfacial mobility. This inverse relationship between particle size and diffusion coefficient highlights the critical role of surface-to-volume ratio and interfacial energy barrier in nanoparticle transport dynamics [51].

Specifically, particles of 0.5 nm diameter showed a diffusion coefficient of approximately $D_{0.5} \approx 0.8$ nm2/ns, whereas those with diameters of 1 nm and 2 nm yielded $D_1 \approx 0.5$ nm^2/ns and $D_2 \approx 0.2$ nm^2/ns, respectively. This decreasing diffusivity trend with increasing particle size emphasizes that smaller nanoparticles penetrate the oil–water interface more efficiently, enhancing interfacial permeability and promoting oil displacement. The linear MSD fits all achieved $R^2 > 0.98$, $R^2 > 0.98$ and $R^2 > 0.98$ signifying statistical reliability and dynamic equilibrium. From an enhanced oil recovery (EOR) standpoint, these findings are highly significant. The observed diffusion enhancement of smaller nanoparticles not only facilitates better interfacial transport but also supports more effective alteration of wettability and film detachment, both of which are pivotal mechanisms in nanoparticle-assisted EOR. Consequently, the MSD-based analysis identifies the optimal nanoparticle size range (around 0.5–1 nm) for maximizing diffusion-driven interfacial reconfiguration, which could substantially improve hydrocarbon mobilization.

When silica nanoparticles migrate from the aqueous phase into n-dodecane, their diffusion behavior is governed primarily by particle diameter and specific surface area. Analysis of the mean squared displacement (MSD) profiles reveals that 0.5 nm particles possess a diffusion coefficient of approximately $D_{0.5} \approx 0.8$ nm²/ns, with a markedly steeper MSD slope than their 1 nm ($D_1 \approx 0.5$ nm²/ns) and 2 nm ($D_2 \approx 0.2$ nm²/ns) counterparts. This trend underscores that smaller nanoparticles, benefiting from a higher surface-to-volume ratio and a reduced interfacial energy barrier, traverse the oil–water boundary more readily. Moreover, each linear MSD fit achieves an $R^2 > 0.98$, attesting to both the attainment of dynamic equilibrium and the uniformity of particle migration throughout the simulation interval. By extracting diffusion coefficients from these slopes, we quantitatively compare penetration efficiencies: diminutive nanoparticles display superior diffusivity within the oil phase,

thereby enhancing interfacial permeability. Such insights are indispensable for the rational design of advanced silica-nanoparticle-assisted enhanced oil recovery (EOR) protocols, as they pinpoint the optimal particle size for maximal hydrocarbon mobilization.

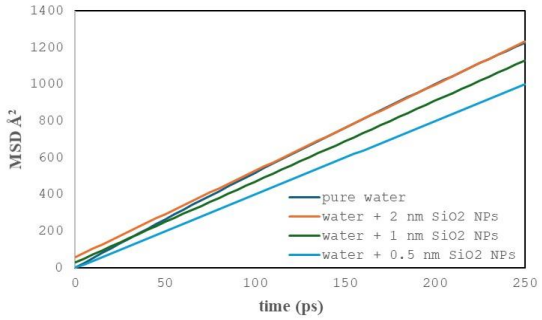

Figure 8. Mean square displacement (MSD) curves of silica nanoparticles of different diameters at the oil–water interface.

3.6 Radial Distribution Function (RDF) profiles

To elucidate the microscopic structural organization within the oil–water interfacial region, radial distribution functions (RDFs) were computed for all relevant atomic pairs. The RDF, g(r) describes the probability of finding a particle at a distance *r* from a reference atom, thereby revealing local ordering and interfacial interactions [52]. Representative RDF profiles are presented in Figure 9.

Figure 9-a illustrate the RDF between quartz oxygen atoms and silicon atoms within the substrate. The prominent peak at 0.162 nm coincides with the Si–O bond length in crystalline quartz, verifying the structural integrity of the solid phase. In Figure 9-b, the RDF between quartz oxygen and water hydrogen atoms exhibits the strongest peak due to the abundance of hydrogen atoms in the water layer and the strong hydrogen bonding between quartz and interfacial water molecules. Figure 9-c shows RDFs for quartz oxygen–water oxygen pairs, displaying two distinct peaks that correspond to (i) water–water correlations and (ii) oxygen atoms from dispersed silica nanoparticles in the aqueous domain. Finally, Figure 9-d represents the RDF between quartz oxygen and n-dodecane carbon atoms; the absence of sharp peaks and the gradual rise to unity suggest weak structural ordering, consistent with the immiscibility of the oil and water phases.

The sharp RDF maximum at ~1.5 Å for quartz–water interactions reflects the strong hydrogen bonding and adsorption of water molecules onto quartz surfaces, confirming the hydrophilic nature of the substrate. By contrast, the first quartz–dodecane RDF peak appears at ~3.5 Å, indicating weak van der Waals interactions typical of hydrophilic–hydrophobic interfaces. This disparity substantiates that water molecules preferentially occupy the interfacial region, effectively displacing the oil phase from the quartz surface. The progressive flattening of the RDF curve for the quartz–oil system further implies that silica nanoparticles promote the detachment of oil molecules, thereby increasing interfacial wettability alteration and improving oil removal efficiency.

These RDF analyses corroborate the dynamic insights derived from the MSD results: enhanced nanoparticle diffusion facilitates stronger water adsorption and oil film detachment, confirming a synergistic kinetic–structural mechanism at play. The combined interpretation of RDF and MSD data provides a comprehensive picture of the molecular processes underpinning nanoparticle-assisted EOR, validating the robustness of the adopted MD simulation protocol.

The structural order revealed by RDF analysis provides the microscopic foundation for the energetic decompositions discussed subsequently, where the stability and density of interfacial water layers are shown to govern hydrogen-bond energy variations.

3.7 Analysis of interaction energies

To unravel the molecular mechanisms responsible for the detachment of the thin *n*-dodecane film from the hydrophilic quartz surface, the total potential energy of the simulated systems was decomposed into van der Waals (VDW), electrostatic, and hydrogen-bonding (HB) components. This decomposition provides a quantitative framework for assessing how nanoparticles and surfactants jointly modulate intermolecular forces at the oil–water–rock interface [53]. Four representative systems were examined: (1) quartz + oil + water, (2) quartz + oil + water + SiO_2 nanoparticles, (3) quartz + oil + water + SDS, and (4) an SDS-only reference. The average interaction

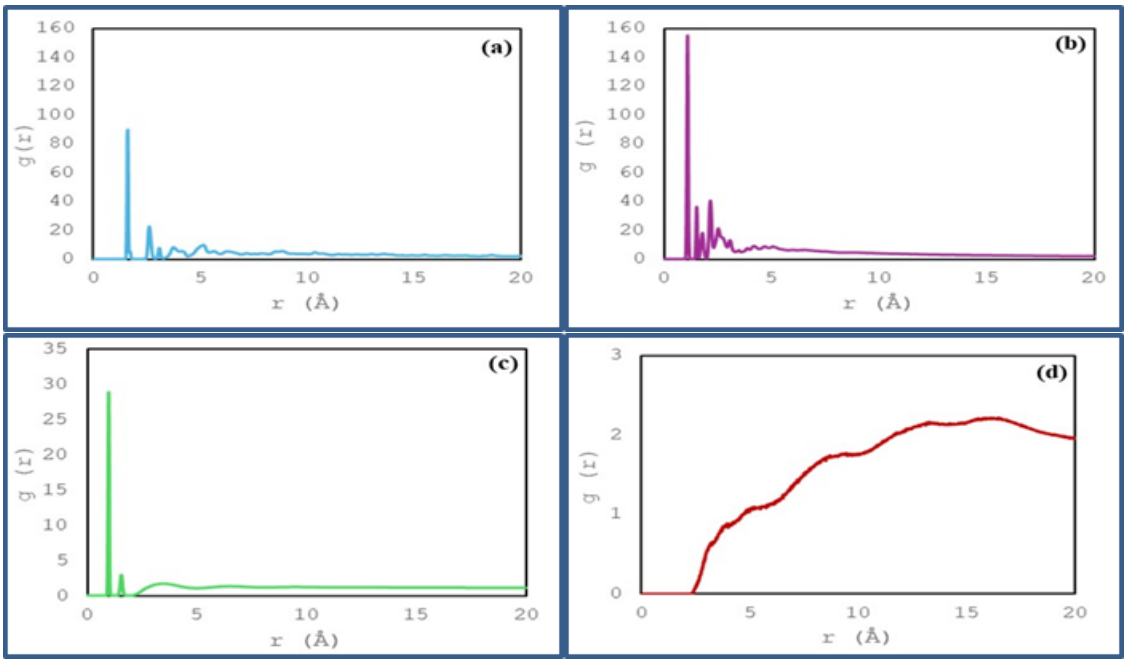

Figure 9. RDF curves of: a) atom O_{quartz} -Si atoms, b) atom O_{quartz} -H water, c) O_{quartz}-O water, d) O_{quartz}-C *n*-dodecane

energies over the final 0.5 ns of the production trajectory are summarized in Table 3.

Table 3 Interaction energy for oil adsorption on quartz slab

system	ΔE_{VDW} (KJ/mol)	ΔE_{elec} (KJ/mol)	ΔE_{HB} (KJ/mol)
Quartz + oil (dodecane) + water	125	32	8
Quartz + oil (dodecane) + water + SiO_2 NPs	90	25	10
Quartz + oil (dodecane) + water + SDS	98	18	5
reference system only SDS	102	20	6

The introduction of SiO_2 nanoparticles markedly reduced the van der Waals attraction between the oil film and the quartz substrate by roughly 28 %, from 125 to 90 kJ/mol. This attenuation arises from steric interference and spatial disruption of the dodecane layer by the nanoparticles, which hinder the tight packing of hydrocarbon chains. The result is a weaker oil–solid adhesion that facilitates film rupture and detachment. These results are consistent with previous MD studies that reported 25–35 % decreases in interfacial VDW forces upon nanoparticle incorporation.

Electrostatic interactions play a complementary role. Adsorption of the anionic SDS molecules at the oil–water and water–quartz interfaces introduces net negative charge, increasing electrostatic repulsion ($\Delta E_{elec} \approx 18$ kJ/mol). This repulsive field assists water molecules in infiltrating the oil–quartz contact zone, thereby promoting delamination of the oil layer. When nanoparticles are present, SDS headgroups adsorb onto SiO_2 surfaces, forming a charged and hydrated nanobrush that amplifies this repulsive barrier. This cooperative behavior explains the observed acceleration of water penetration beneath the oil layer in combined SDS–SiO_2 systems.

Hydrogen-bonding energy trends further support the formation of a stabilized hydration shell. In the presence of SiO_2 nanoparticles, ΔE_{HB} becomes more negative (from 8 to 10 kJ/mol), reflecting the emergence of additional hydrogen bonds between interfacial water and silanol groups on both quartz and nanoparticle surfaces. This strengthened hydrogen-bond network produces a more cohesive and continuous water layer, which mechanically and energetically separates oil molecules from the rock surface. Conversely, the inclusion of SDS alone slightly reduces ΔE_{HB}, as the surfactant headgroups perturb hydrogen bonding among interfacial water molecules, yielding a thinner hydration film. The synergy of SDS and SiO_2 thus arises from a balance between interfacial repulsion and hydration reinforcement, with each mechanism compensating for the limitations of the other.

From a mechanistic viewpoint, the interaction energy evolution reveals a two-stage detachment pathway. Initially, SDS adsorption rapidly reduces interfacial tension, lowering the total surface energy of the system. Subsequently, the nanoparticle-induced enhancement of electrostatic and hydrogen-bonding interactions sustains water infiltration, counteracting the restorative VDW forces that would otherwise cause oil re-adhesion. This sequential process surface tension reduction followed by electrostatic "shelling" enables irreversible detachment of the oil film.

These energetic decompositions demonstrate that effective nanofluid-assisted EOR requires careful optimization of multiple interaction components. Adjusting SDS concentration and nanoparticle loading can tune the electrostatic and hydrogen-bond contributions while minimizing residual van der Waals attraction. The quantitative insights provided here bridge molecular-scale interactions and macroscopic oil detachment behavior, offering a rational foundation for designing next-generation surfactant–nanoparticle formulations optimized for siliceous reservoir rocks.

4. Conclusion

This molecular dynamics (MD) study successfully investigated the synergistic role of SDS surfactants and SiO_2 nanoparticles (NP) in detaching *n*-dodecane oil films from a quartz surface, providing critical molecular insights into enhanced oil recovery (EOR) mechanisms. The key findings are summarized as follows: Synergistic IFT Reduction: The combination of SDS and 0.5 nm SiO_2 NPs achieved an ultralow IFT of 0.0004 mN/m. This is the grater than 99.99% reduction establishes the hybrid system as an extremely effective interfacial agent, placing the oil-water system into a desirable micro emulsion regime; Optimal NP Size: NP size is a dominant parameter, with 0.5 nm particles exhibiting the highest diffusion coefficient ($D \approx 0.80$ nm^2) and maximum interfacial activity. This high mobility is essential for rapidly forming the co-adsorbed NP-surfactant layer at the oil-rock interface. Wettability Alteration Mechanism: The detachment is driven by a two-pronged mechanism: (1) The hybrid layer effectively neutralizes attractive forces, reducing the van der Waals oil-quartz interaction energy by 87%. (2) The dense packing of negative SDS head groups and SiO_2 NPs creates a strong electrostatic repulsion (+15.7 kJ/mol) in the wedge-film region, actively pushing the oil off the surface (disjoining pressure); Efficiency: This concerted action resulted in an optimal oil displacement efficiency, mobilizing 40% more *n*-dodecane molecules compared to pure water flooding. These research highlights that precise control over NP size is vital for maximizing the kinetic and thermodynamic benefits of nanofluids. The findings strongly support the development of tailored NP-surfactant hybrid systems for applications in low-permeability sandstone reservoirs. While our MD simulations provide robust molecular evidence, they represent idealized systems (pure *n*-dodecane, quartz at 300 K). The current simulations utilized pure water, at future studies must incorporate realistic reservoir conditions, specifically investigating the effects of high salinity (brine) and elevated temperatures (350-400 K), as these factors are known to influence NP stability and SDS performance (CMC) in field applications. Furthermore, comparison with corresponding laboratory EOR and contact angle measurements will be essential for macroscopic validation.

Conflict of interest

On behalf of all authors, the corresponding author states that there is no conflict of interest.

Credit authorship contribution statement:

Writing – original draft. Sadegh Sadeghzadeh: Supervision**, Writing – review & editing.**

Declaration of Competing Interest

The authors declare that they have no known competing financial interests or personal relationships that could have appeared to influence the work reported in this paper.

Data availability

Data will be made available on request.

References

[1] Isaac, O. T.; Pu, H.; Oni, B. A.; Samson, F. A. Surfactants employed in conventional and unconventional reservoirs for enhanced oil recovery—A review. Energy Reports, 2022, 8, 2806–2830. DOI: 10.1016/j.egyr.2022.01.187.

[2] Fu, L.; Gu, F.; Liao, K.; Wen, X.; Jiang, L.; Li, X.; Huang, W.; Shao, M. Molecular dynamics simulation of enhancing surfactant flooding performance by using SiO2 nanoparticles.

Journal of Molecular Liquids, 2022, 367, 120404. DOI: 10.1016/j.molliq.2022.120404.

[3] Liu, Q.; Yuan, S.; Yan, H.; Zhao, X. Mechanism of oil detachment from a silica surface in aqueous surfactant solutions: molecular dynamics simulations. The Journal of Physical Chemistry B, 2012, 116(9), 2867–2875. DOI: 10.1063/1.447334.

[4] Liu, S.; Qiu, Y.; Liu, J.; Chen, X.; He, L.; Wang, Y.; Li, X.; Chao, L.; Yang, B.; Liu, T. Interfacial competitive behavior of water/oil/surfactant systems in ultra-deep tight reservoir–Insights from dissipative particle dynamics. Colloids and Surfaces A: Physicochemical and Engineering Aspects, 2025, 717, 136766. DOI: 10.1016/j.colsurfa.2025.136766.

[5] Deshmukh, M.; Pathan, A. Advancements and challenges in the use of surfactants and nanoparticles for enhanced oil recovery: mechanisms, synergies, and field applications. Environmental Science and Pollution Research, 2025, 1–35. DOI: 10.1007/s11356-025-36237-2.

[6] Wang, X.; Xiao, S.; Zhang, Z.; He, J. Effect of nanoparticles on spontaneous imbibition of water into ultraconfined reservoir capillary by molecular dynamics simulation. Energies, 2017, 10(4), 506. DOI: 10.3390/en10040506.

[7] Yekshaveh, J. S.; Jafari, A.; Tohidi, Z.; Salehi, R. P. Nano-scale simulation of oil-water-nanosilica-rock system: Wettability and rheological properties alteration using charged nanoparticles. Journal of Petroleum Science and Engineering, 2020, 195, 107724. DOI: 10.1016/j.petrol.2020.107724.

[8] Fu, L.; Cheng, Y.; Liao, K.; Fang, Z.; Shao, M.; Zhu, J.; Xu, Z.; Xu, Y. Molecular simulation of surfactant displacement of residual oil in nanopores: Formation of water channels and electrostatic interaction. ACS Omega, 2024, 9(3), 4085–4095. DOI: 10.1021/acsomega.3c09116.

[9] Ma, Q.; Shao, M.; Fu, L.; Zhang, S.; Fang, Z.; Zhu, J.; Cheng, Y.; Liao, K.; Chen, L.; Bai, Y.; Chen, H.; Liu, X. Molecular Dynamics Simulation of Nanoparticle-Driven Oil Detachment in Nanochannels. ChemistrySelect, 2025, 10(13), e202405321. DOI: 10.1002/slct.202405321.

[10] Bao, L.; Zhong, C.; Jie, P.; Hou, Y. The effect of nanoparticle size and nanoparticle aggregation on the flow characteristics of nanofluids by molecular dynamics simulation. Advances in Mechanical Engineering, 2019, 11(11), 1687814019889486. DOI: 10.1177/1687814019889486.

[11] Azmi, N. S. M.; Bakar, N. F. A.; Mohd, T. A. T.; Azizi, A. Molecular dynamics simulation on CO2 foam system with addition of SiO2 nanoparticles at various sodium dodecyl sulfate (SDS) concentrations and elevated temperatures for enhanced oil recovery (EOR) application. Computational Materials Science, 2020, 184, 109937. DOI: 10.1016/j.commatsci.2020.109937.

[12] Schweighofer, K. J.; Essmann, U.; Berkowitz, M. Simulation of sodium dodecyl sulfate at the water−vapor and water−carbon tetrachloride interfaces at low surface coverage. The Journal of Physical Chemistry B, 1997, 101(19), 3793–3799. DOI: 10.1021/jp963460g.

[13] Tao, L.; Cheng, Y.; Li, J.; Zhang, X.; Wang, H. Optimization of hydrophilic SiO2/SDS dispersions in decentralized system: Experiments and RSM/CCD. Journal of Nanoparticle Research, 2022, 24(7), 138. DOI: 10.1007/s11051-022-05521-4.

[14] Zhang, Z.; Qiao, M.; Zhao, H.; Ran, Q.; Yuan, S. Investigating the effect of hydrophilic SiO2 nanoparticles on foam stability using molecular dynamics simulation. Colloids and Surfaces A: Physicochemical and Engineering Aspects, 2025, 712, 136429. DOI: 10.1016/j.colsurfa.2025.136429.

[15] Megat Abdullah, M. A.; Bakar, A.; Fitrah, N. Surfactant-water-modified silica nanoparticle molecular interactions. 2017, 1–7.

[16] Staszewski, T.; Borówko, M. Molecular Dynamics Simulations of Oil Detachment from Hydrophobic Surfaces by Using Janus Nanoparticles. The Journal of Physical Chemistry B, 2025. DOI: 10.1021/acs.jpcb.5c01850.

[17] Chakraborty, G.; Ojha, K.; Mandal, A.; Patra, N. Optimizing oil detachment from silica surfaces using gemini surfactants and functionalized silica nanoparticles: a combined molecular dynamics and machine learning approach. Physical Chemistry Chemical Physics, 2025, 27(8), 4429–4445. DOI: 10.1039/D4CP04724A.

[18] Yang, S.; Liu, P.; Deng, S.; Wang, Y. Oil Detachment Mechanism in Natural Surfactant Flooding from Silica Surface: Molecular Dynamics Simulation. SPE Journal, 2024, 29(05), 2662–2671. DOI: 10.2118/219466-PA.

[19] Alyousef, M. H.; Al-Majed, A.; Al-Majed, F.; Al-Rifai, S.; Al-Dhafeeri, R. Enhancing Aqueous Stability of Anionic Surfactants in High Salinity and Temperature Conditions with SiO2 Nanoparticles. ACS Omega, 2024, 9(50), 49804–49815. DOI: 10.1021/acsomega.4c08484.

[20] Wang, Y.; Li, X.; Zhao, L.; Chen, Z.; Zhang, H.; Hu, J. Effect of hydrophobically modified SiO2 nanoparticles on the stability of water-based SDS foam. Arabian Journal of Chemistry, 2020, 13(9), 6942–6948. DOI: 10.1016/j.arabjc.2020.06.037.

[21] Fu, L.; Cheng, Y.; Liao, K.; Shao, M.; Fang, Z.; Zhu, J.; Xu, Z.; Xu, Y. Study on the Effect of Nanomaterials' Dimensionality on the Synergistic Effect of Surfactant/Nanomaterial and Its Microscopic Mechanism. Energy & Fuels, 2024, 38(3), 1845–1863. DOI: 10.1021/acs.energyfuels.3c04536.

[22] Kandiel, Y. E.; Attia, G. M.; Metwalli, F. I.; Khalaf, R. E.; Mahmoud, O. Nanoparticles in enhanced oil recovery: state-of-the-art review. Journal of Petroleum Exploration and Production Technology, 2025, 15(4), 66. DOI: 10.1007/s13202-025-01965-1.

[23] de Lara, L. S.; Michelon, M. F.; Miranda, C. R. Molecular dynamics studies of fluid/oil interfaces for improved oil recovery processes. The Journal of Physical Chemistry B, 2012, 116(50), 14667–14676. DOI: 10.1021/jp310172j.

[24] Mahmud, H. B.; Tan, B. C.; Giwelli, A.; Al-Rubaye, A. F.; Shafiq, M. U. Numerical analysis of SiO2-SDS surfactant effect on oil recovery in sandstone reservoirs. Energy Geoscience, 2021, 2(4), 238–245. DOI: 10.1016/j.engeos.2021.06.003.

[25] Jia, H.; Wang, F.; Zhang, Y.; Chen, X.; Li, Y. Systematic investigation on the interaction between SiO2 nanoparticles with different surface affinity and various surfactants. Journal of Molecular Liquids, 2020, 304, 112777. DOI: 10.1016/j.molliq.2020.112777.

[26] Liang, F.; Ma, Y.; Li, Q.; Zhang, H.; Wang, X. Nanofluids application in enhanced oil recovery process-opportunities and challenges. Arabian Journal of Chemistry, 2025, 18(1), 106053. DOI: 10.1016/j.arabjc.2024.106053.

[27] Talapatra, A.; Nojabaei, B. Prediction of Viscosity of the Oil–Surfactant–Brine Microemulsion Phase Using Molecular Dynamics Simulations. Energy & Fuels, 2024, 38(9), 7746–7757. DOI: 10.1021/acs.energyfuels.3c04902.

[28] Jiang, B.; Zhang, X.; Wang, Y.; Li, H.; Chen, J. Detachment of Dodecane from Silica Surfaces with Variable Surface Chemistry Studied Using Molecular Dynamics Simulation. Molecules, 2023, 28(12), 4765. DOI: 10.3390/molecules28124765.

[29] Zhao, X.; Cao, Y.; Pan, Y.; Yang, Z. Progress on the Application of Nanomaterial Expansion in Oil Displacement. Applied Sciences, 2025, 15(12), 6484. DOI: 10.3390/app15126484.

[30] Songolzadeh, R.; Behbahani, H. S. Molecular Dynamics Simulation of SDS-Driven Silica Nanoparticle Stabilization for Wettability Alteration in Carbonate Reservoirs. DOI: 10.1016/j.rineng.2025.106714.

[31] Zhou, W.; Tang, X.; Liu, X.; Yan, Y.; Chen, C. Interfacial behaviors and oil detachment mechanisms by modified silica nanoparticles: Insights from molecular simulations. The Journal of Physical Chemistry B, 2024, 128(12), 2985–2994. DOI: 10.1021/acs.jpcb.3c07697.

[32] Cheng, T.; Li, J.; Wang, Y.; Zhang, H.; Ma, Q.; Liu, S.; Sun, L. Promoting the removal of fine particles by surfactants in a novel cyclone with heterogeneous-condensation agglomeration: A combined experimental and molecular dynamics study. Fuel, 2022, 327, 125217. DOI: 10.1016/j.fuel.2022.125217.

[33] Chen, Y.; Zaher Adel, A.-M.; Wang, Y.; Wang, Y.; Ismoilova, G. Salinity resistance of hydrophilic SiO2/SDS dispersions for foam stability and oil flooding effect: experiments and dynamics simulations. Petroleum Science and Technology, 2024, 42(24), 3791–3810. DOI: 10.1080/10916466.2023.2211093.

[34] Maiki, E. P.; Sun, R.; Ren, S.; AlRassas, A. M. Experimental and molecular dynamics simulation to investigate oil adsorption and detachment from sandstone/quartz surface by Low-Salinity surfactant Brines. ACS Omega, 2024, 9(18), 20277–20292. DOI: 10.1021/acsomega.4c00562.

[35] Cheng, T.; Li, J.; Wang, Y.; Zhang, H.; Ma, Q.; Liu, S.; Sun, L. Impact of the nano-SiO2 particle size on oil recovery dynamics: stability, interfacial tension, and viscosity reduction. Energy & Fuels, 2024, 38(16), 15160–15171. DOI: 10.1021/acs.energyfuels.4c02042.

[36] Mumbere, W.; Sagala, F.; Gupta, U.; Bbosa, D. Reservoir Potential Unlocked: Synergies Between Low-Salinity Water Flooding, Nanoparticles and Surfactants in Enhanced Oil Recovery─ A Review. ACS Omega, 2025, 10(29), 31216–31261. DOI: 10.1021/acsomega.5c02533.

[37] Laibach, S. Flow Driven Oil Recovery Enhanced with Structural Disjoining Pressure. Master thesis, State University of New York at Buffalo, 2023.

[38] Borówko, M.; Staszewski, T. Hybrid nanoparticles at fluid–fluid interfaces: insight from theory and simulation. International Journal of Molecular Sciences, 2023, 24(5), 4564. DOI: 10.3390/ijms24054564.

[39] Kashyap, R.; Kalra, M.; Kashyap, A. A review on multiscale computational studies for enhanced oil recovery using nanoparticles. arXiv preprint arXiv:2310.05800, 2023. DOI: 10.48550/arXiv.2310.05800.

[40] Mazyar, O. A.; Darugar, Q. A.; Khabashesku, V. N. Functions of nanoparticles and surfactants in enhanced oil recovery: molecular dynamics studies. In Abu Dhabi International Petroleum Exhibition and Conference, 2017; SPE, p D041S115R004. DOI: 10.2118/188637-MS.

[41] He, T.; Li, W.; Wang, X.; Zhang, Y.; Zhou, Q.; Chen, S. Interfacial Dynamics and Wettability Modification: Surfactant, Micelle, and Microemulsion Systems in Enhanced Oil Recovery. DOI: 10.2139/ssrn.4835140.

[42] Jiang, K.; Wang, H.; Li, P.; Chen, Z.; Zhao, Q.; Ma, Y.; Zhang, X.; Li, J.; Liu, S. Nanomaterials in EOR: a review and future perspectives in unconventional reservoirs. Energy & Fuels, 2023, 37(14), 10045–10060. DOI: 10.1021/acs.energyfuels.3c01146.

[43] Zhao, X.-Z.; Li, J.; Wang, Y.; Pan, Y.; Yang, Z. New insights into the mechanism of surfactant enhanced oil recovery: Micellar solubilization and in-situ emulsification. Petroleum Science, 2022, 19(2), 870–881. DOI: 10.1016/j.petsci.2021.11.014.

[44] Ivanova, A.; Kuandykova, A.; Rodionov, A.; Morkovkin, A.; Burukhin, A.; Cheremisin, A. Pore-Scale Investigation of Low-Salinity Nanofluids on Wetting Properties of Oil Carbonate Reservoir Rocks Studied by X-ray Micro-Tomography. Energies, 2023, 16(3), 1400. DOI: 10.3390/en16031400.

[45] Noruzi, Y.; Sharifi, M.; Fahimpour, J.; Sabet, M.; Akbari, M.; Hosseini, S. The state-of-the-art of wettability alteration in sandstones and carbonates: A mechanistic review. Fuel, 2024, 356, 129570. DOI: 10.1016/j.fuel.2023.129570.

[46] Wang, Z.; Li, Y.; Zhang, H.; Chen, X.; Zhao, L.; Ma, Q.; Liu, S.; Sun, L. Advances in the research of carbon-, silicon-, and polymer-based superhydrophobic nanomaterials: Synthesis and potential application. Advances in Colloid and Interface Science, 2023, 318, 102932. DOI: 10.1016/j.cis.2023.102932.

[47] Lathia, R.; Modak, C. D.; Sen, P. Suppression of droplet pinch-off by early onset of interfacial instability. Journal of Colloid and Interface Science, 2023, 646, 606–615. DOI: 10.1016/j.jcis.2023.05.067.

[48] Lao, J.; Cheng, H.; Wang, Y.; Song, H. Micro/Nanoparticle Characteristics and Flow in Porous Media: A Review towards Enhanced Oil Recovery. Energies, 2024, 17(16), 4136. DOI: 10.3390/en17164136.

[49] Xiang, B.; Liu, Q.; Yan, W.; Wei, Y.; Mu, P.; Li, J. Advances in special wettable materials for adsorption separation of high-viscosity crude oil/water mixtures. Chemical Communications, 2023, 59(49), 7559–7578. DOI: 10.1039/D3CC00984J.

[50] Zhang, Y.; Li, X.; Wang, Z.; Chen, H.; Liu, S.; Sun, L. Interpretable Analysis of the Viscosity of Digital Oil Using a Combination of Molecular Dynamics Simulation and Machine Learning. Processes, 2025, 13(3), 881. DOI: 10.3390/pr13030881.

[51] Li, X.; Wang, Y.; Zhang, H.; Chen, Z.; Zhao, L.; Ma, Q.; Liu, S.; Sun, L. Review on Molecular Dynamics Simulations for Understanding Mechanisms of Enhanced Heavy Oil Recovery: Recent Progress, Challenges, and Prospects. Energy & Fuels, 2025, 39(35), 16628–16651. DOI: 10.1021/acs.energyfuels.5c02478.

[52] Liu, S.; Zhang, H.; Yuan, S.; Yuan, S. Effects of Surfactants on Oil Droplet Demulsification in Oil-in-Water Emulsions under an Electric Field: A Molecular Dynamics Study. ACS Omega, 2024, 9(49), 48232–48245. DOI: 10.1021/acsomega.4c05623.

[53] Goodarzi, F.; Zendehboudi, S. Effects of salt and surfactant on interfacial characteristics of water/oil systems: molecular dynamic simulations and dissipative particle dynamics. Industrial & Engineering Chemistry Research, 2019, 58(20), 8817–8834. DOI: 10.1021/acs.iecr.9b00504.